Biosensors and Bioelectronics 145 (2019) 111713

Contents lists available at ScienceDirect

Biosensors and Bioelectronics

journal homepage: www.elsevier.com/locate/bios

A graphene oxide-gold nanostar hybrid based-paper biosensor for label-free SERS detection of serum bilirubin for diagnosis of jaundice

Xiang Pan, Linhu Li, Hangduo Lin, Jiayi Tan, Haitao Wang, Mengling Liao, Caiju Chen, Beibei Shan, Yingfan Chen, Ming Li*

School of Materials Science and Engineering, Central South University, Changsha, Hunan, 410083, China

ARTICLE INFO

Keywords:
Free bilirubin
Surface-enhanced Raman spectroscopy
Jaundice
Graphene oxide
Plasmonic gold nanostar

ABSTRACT

We report a paper-based surface-enhanced Raman spectroscopy (SERS) biosensor integrating the enrichment capability, namely enPSERS biosensor, for the sensitive, label-free detection of free bilirubin in blood serum for the accurate diagnosis of jaundice and its related diseases. This biosensor comprises multifunctional graphene oxide-plasmonic gold nanostar (GO-GNS) hybrids decorated on the filter paper, which integrates the high sensitivity of SERS detection, enrichment for serum bilirubin and fluorescence superquenching capability of GO-GNS hybrids for sensitive detection of serum bilirubin. The study of adsorption kinetics reveals that both electrostatic and π-π interactions between the GO-GNS hybrids and targets are responsible for the enrichment of bilirubin, and the adsorption process follows the pseudo-second-order kinetic model. The results of SERS detection of bilirubin in blood serum show two differential linear response ranges from 5.0 to 150 μM and 150–500 μM with the detection limit as low as 0.436 μM. The comparison of the results obtained from our present enPSERS biosensor with the commercial diazo reaction method for determination of free bilirubin in blood serum reveals the clinical effectiveness and suitability of the developed paper-based SERS biosensor. We believe that this sensitive and label-free SERS biosensor holds considerable promise for clinical translation in accurate diagnosis of jaundice.

1. Introduction

Jaundice continues to be a serious health concern and is among the leading causes of deaths during the first days of newborn babies' lives (Olusanya et al., 2018; Bonnett et al., 1976). Serum bilirubin is currently being exploited in the clinic as a key biomarker for the diagnosis and management of neonatal jaundice. Bilirubin is the breakdown product of heme proteins formed in the heme catabolism. It normally exists as a free (unconjugated) form of a lipophilic nature in human blood but can bind to human serum albumin to form a water-soluble complex, eventually excreted into the bile (Brodersen and Stern, 1980; Hooda et al., 2017). Free bilirubin in blood serum is generally unexcretable and toxic to human body; high level of free bilirubin (called hyperbilirubinemia) in serum may evoke hepatic or biliary tract dysfunction, mental disorders, permanent brain damage especially in neonates, even death in more severe cases (Berthelot et al., 2018). In general, the normal level of free bilirubin is $< 25\,\mu M$ ($< 12\,mg/L$) in healthy human blood but it is increased to $> 50\,\mu M$ ($> 25\,mg/L$) under jaundice condition (Hooda et al., 2017; Silbernagl and Despopoulos, 2009). Disorders in the metabolism of bilirubin may lead to some symptoms — yellowish discoloration of the skin and eyes, dark yellow urine, headache, weight loss, fatigue, drowsiness and (or) low appetite (Brito et al., 2006; Subbiah and West, 2016). Thus, uncontrolled or rapidly rising level of free bilirubin in serum could potentially cause lethal consequences if not appropriately treated. Therefore, there is a pressing need to monitor the concentration of free bilirubin in human serum for diagnosing jaundice and hyperbilirubinemia-induced disorders.

The gold standard method for measuring free bilirubin in serum samples is high-performance liquid chromatography (HPLC) because it is not subject to interference from other heme proteins (Bhutani et al., 2003). However, this method is labor-intensive and not practical for clinical use. Currently, the commonly used methods for serum bilirubin determination in clinical settings are direct spectroscopic measurement and the diazo reaction method (Kazmierczak et al., 2002; Batra et al., 2013; Hajzer, 1989; Hutchinson et al., 1972). However, direct spectroscopic measurement usually suffers from interference with other heme proteins existing in blood serum while the pH dependence of the

* Corresponding author.
E-mail addresses: liming0823@csu.edu.cn, liming0823@gmail.com (M. Li).

https://doi.org/10.1016/j.bios.2019.111713
Received 5 August 2019; Received in revised form 16 September 2019; Accepted 17 September 2019
Available online 17 September 2019
0956-5663/

diazo reaction compromises the accuracy of the diazo method. Other alternative methods for bilirubin detection include bilirubin oxidase based enzymatic assay (Doumas et al., 1987), vanadate oxidation assay (Ameri et al., 2011), polarography (Zeng et al., 1994), colorimetric method (Rolinski et al., 2001), fluorimetric method (Ellairaja et al., 2017; Du et al., 2017), capillary electrophoresis and electrochemical method (Batra et al., 2013; Thangamuthu et al., 2018; Rahman et al., 2008). Drawbacks such as low sensitivity, high-cost, toxic chemicals and low-stability of bilirubin oxidase limit the use of the bilirubin oxidase method under ambient conditions. Additionally, other methods have limitations regarding expensive instrumentation, tedious sample preparation, high cost, professional training, less specificity, etc. To address unmet demands, it is very urgent to develop a rapid and economical route for sensitive and specific detection of free bilirubin directly in human serum.

Surface-enhanced Raman spectroscopy (SERS) has gained considerable attention as a potent analytical tool in biomedical applications owing to its near single-molecule detection sensitivity, powerful multiplex capability and excellent photostability (Shan et al., 2018; Li et al., 2015a; Stiles et al., 2008; Wang et al., 2012, 2017). By exploiting the electromagnetic field confinement effect resulting from the excitation of the localized surface plasmon resonance (LSPR) in noble-metallic nanostructures, SERS signals of Raman molecules in close proximity to the plasmonic nanostructures can be dramatically enhanced with sensitivity down to femtomolar concentrations (Shan et al., 2018; Li et al., 2015a). More importantly, SERS is a truly label-free technique, in that it provides intrinsic SERS signals of biomarkers of interest directly in complex biological matrices and does not require any label or special treatment of the SERS substrates and samples. These advantages enable SERS detection as an ideal alternative for sensitive and accurate detections of serum bilirubin. It is logically realized that the plasmonic substrates are paramount in obtaining high performance SERS biosensing. In the past decades, much of the development effort of SERS biosensing has been focused on innovating a variety of plasmonic nanostructures with high SERS enhancement factor (EF), with the aim of improving the detection sensitivity (Li et al., 2012a, 2017; Rycenga et al., 2011; Pu et al., 2018; Wei et al., 2009; Brolo et al., 2004). Anisotropic nanostructures with "built-in" hot-spots including nanorods, nanocubes, nanostars, nanotriangle plates and nanoflowers are more attractive SERS substrates because of their high SERS enhancement capability without the need for complicated manipulation that is usually used to achieve hot-spots (Shan et al., 2018). Considering the extremely low concentrations of biomarkers in clinical samples, the design strategy of biosensors for the detection in real samples requires the pre-concentration of biomarkers during the implementation of SERS measurements, in addition to the large SERS enhancement by SERS substrates. Previous studies integrated polymers or magnetic nanostructures with SERS substrates for simultaneous enrichment and plasmonic enhancement of the analytes, achieving excellent SERS detection performance for biomarkers of pathological significance (Bai et al., 2019; Zhang et al., 2012; Han et al., 2013; Zhou et al., 2016; Yuan et al., 2018). In addition, it is widely reported that graphene and its graphene oxide (GO) derivatives have been considered as excellent drug carriers with extremely high drug loading capacity because of its large surface area, low manufacturing cost, strong π-π and electrostatic interactions (Panikar et al., 2018; Wang et al., 2015; Chen et al., 2015, 2016; Qiu et al., 2017; Fan et al., 2013; Lu et al., 2011). Also, both charge-transfer induced chemical enhancement for SERS and superquenching capability toward fluorescence were observed in graphene and GO. Coating or hybridization of plasmonic nanoparticles with graphene or GO nanosheets have been demonstrated for high performance SERS sensing in the literature (Yu et al., 2011; Xu et al., 2012). Therefore, the rational combination of plasmonic noble-metallic (i.e., Au, Ag) nanostructures with GO could provide a particularly promising platform for sensitive SERS detection of serum bilirubin with molecular specificity.

In this work, we develop a paper-based SERS biosensor integrating the enrichment capability, namely enPSERS biosensor, for sensitive, label-free detection of serum bilirubin for the jaundice diagnosis. The enPSERS biosensor combines the enrichment for serum bilirubin and plasmonic enhancement for Raman signals of bilirubin for boosting the label-free detection sensitivity directly in blood serum without the need for additional sample preparation. The critical component of the enPSERS biosensor is the graphene oxide-plasmonic gold nanostar (GO-GNS) hybrids densely coated onto the filter paper. The plasmonic GNSs are employed for the SERS enhancement because of its ultrahigh EF and built-in "hot-spots", as studied in detail in our previous work (Li et al., 2012c, 2013a, 2014; Pu et al., 2018). Rather than the direct growth method, the physical self-assembly between the GO nanosheets and plasmonic GNSs was adopted for the preparation of GO-GNS hybrids. The physical self-assembly method makes excellent control over the deposition of colloidal GNSs onto the GO nanosheets, and preserves the initial morphology and high SERS activity of GNSs as well as the adsorption properties of GO nanosheets. In the present design, three key features contribute to the high-performance of the enPSERS biosensor: (i) the bilirubin enrichment through the strong electrostatic and π-π interactions between the GO nanosheet and the bilirubin targets, (ii) the superquenching of fluorescence by both GO nanosheets and GNSs, and (iii) the high SERS activity of plasmonic GNSs. The developed enPSERS biosensor provides advantages over conventional methods such as high sensitivity and specificity, simple operation, rapid response, low cost and reliability, for label-free SERS detection of free bilirubin in blood serum. We expect that the present enPSERS biosensor has great potential to serve as a powerful tool for the jaundice diagnosis in clinical translation.

2. Materials and methods

2.1. Chemicals and materials

Graphene oxide (GO, > 99%) was obtained from Nanjing JCNANO Tech Co., Ltd. (Nanjing, China). Poly(vinylpyrrolidone) (PVP, $(C_6H_9NO)_n$, M.W. ≈ 10 kg/mol) and trypan blue solution (TP, 0.4%) were purchased from Sigma-Aldrich Shanghai Trading Co., Ltd. (Shanghai, China). Trisodium citrate dihydrate ($HOC(COONa)(CH_2COONa)_2{\cdot}2H_2O$, analytical reagent), potassium chloride (analytical reagent), sodium borohydride (≥98%) and *N*,*N*-dimethylformamide (DMF, anhydrous 99.8%) were purchased from Sinopharm Chemical Reagent Co., Ltd. (Beijing, China). Chloroauric acid ($HAuCl_4{\cdot}4H_2O$, 99% trace metals basis) was ordered from Shanghai Civi Chemical Technology Co., Ltd. (Shanghai, China). Gold standard solution (1000 μg/mL) was obtained from Guobiao (Beijing) Testing & Certification Co., Ltd. (Beijing, China). Bilirubin (> 98%) and methylene blue (MB) were purchased from Aladdin Chemistry Co., Ltd. (Shanghai, China). Chemical analysis filter paper (Φ = 7 cm) was obtained from Hangzhou Special Paper Industry Co., Ltd. (Hangzhou, China). Poly(diallyldimethyl ammonium chloride) (PDDA, M.W. ≈ 100 kg/mol) and 4-nitrothiophenol (4-NTP, > 90%) were purchased from Shanghai Macklin Biochemical Technology Co., Ltd. (Shanghai, China). The bilirubin assay kit was obtained from Biosino Bio-Technology and Scientific Incorporation (Beijing, China). Fetal bovine serum (FBS) was provided by Biological Industries Co., (Haemek, Israel). Ultrapure water (18.2 MΩ cm@25 °C) was produced with a Millipore Direct-Q3 UV system (Millipore Corporation, Molshein, France) and used throughout all experiments. All of chemicals and solvents were of analytical grade and used as received. All glassware used in this work was cleaned with aqua regia, rinsed thoroughly with ultrapure water and then air-dried prior to use throughout all experiments.

2.2. Characterization and instrumentation

Zeta potential measurements were taken on a Malvern Zetasizer Nano-ZS ZEN3600 analyzer (Malvern Instrument Ltd., UK). The absorption spectra were recorded in the wavelength range of 200–1100 nm on an Agilent Cary 5000 UV–vis–NIR spectrophotometer (Agilent Technology, USA). Transmission electron microscopy (TEM) images were acquired on an FEI Tecnai G2 F20 field emission instrument (FEI, USA) operating at 200 kV. Samples were prepared by drying a drop of the colloidal suspension on a thin carbon-coated 300 mesh copper grid (Beijing Zhongjingkeyi Technology Co. Ltd., China). Size distribution of GNSs was statistically determined from the TEM data using the ImageJ analysis software. Inductively coupled plasma-optical emission spectroscopy (ICP-OES) measurements were carried out on an Agilent 5100 inductively coupled plasma-optical emission spectrometer (Agilent Technologies, USA). The ICP-OES samples were thoroughly washed with ultrapure water, and then digested by aqua regia to obtain a clear solution. The diazo reaction measurements for total bilirubin quantification were performed in a 96-well microplate on a Tecan Spark microplate reader (Männedorf, Switzerland).

2.3. Preparation of the enPSERS biosensor

GNSs were synthesized using a seed-mediated growth method previously reported by our group (Li et al., 2014; Pu et al., 2018). The LSPR wavelength of GNSs was tuned to lie at 778 nm by changing the gold seed/$AuCl_4^-$ ratio, which possesses a large SERS EF under the laser excitation of 785 nm (Li et al., 2014). The concentration of GNS suspensions was determined to be 0.225 mg/mL by ICP-OES.

Co-modification of GO Nanosheets with PVP and PDDA. GO nanosheets were co-modified with PVP and PDDA according to the well-established protocols described in the literature (Fang et al., 2010). Firstly, PVP-modified GO (PVP-GO) was prepared by adding 96 mg PVP to 24 mL of 0.5 mg/mL GO aqueous suspension. After stirring for 12 h, the reaction mixture was washed with ultrapure water, and the resulting product is the PVP-GO, which was re-dispersed into 12 mL ultrapure water. Following this, PVP-GO was further functionalized by PDDA. Briefly, 3 mL of 1.0 mg/mL PVP-GO suspension was added to 12 mL of the aqueous solution containing 0.625 M KCl and 1.25 mg/mL PDDA. After sonication for 3 h, the suspension was centrifuged and washed at least twice with ultrapure water to remove excess PDDA. The resulting PDDA-GO was re-dispersed in 6 mL ultrapure water.

Preparation of GO-GNS Hybrids. PDDA-GO (67 μg/mL) was added under magnetic stirring to 1.5 mL of aqueous solutions containing the GNS concentrations of 75, 93.8, 112.5, 150, 187.5 and 225 μg/mL. After sonication for 2 min the reaction mixture was kept still overnight, followed by thoroughly washing with ultrapure water. The resulting GO-GNS hybrids were re-dispersed into 1 mL ultrapure water. The GNS:GO mass ratios (m_{GNS}/m_{GO}) in these GO-GNS hybrids are 24 ± 2%, 61 ± 1%, 79 ± 1%, 99 ± 1%, 110 ± 1%, 121 ± 2%, determined by ICP-OES.

Preparation of the enPSERS Biosensor. The chemical analysis filter paper was cut into discs with a diameter of 5 mm, and then 40 μL of the GO-GNS hybrid suspension was dropped onto the paper, followed by drying at 30 °C in a vacuum oven. The resulting paper is the enPSERS biosensor.

2.4. SERS detection of bilirubin

SERS measurements were performed with a Renishaw inVia Raman microscope system coupled with a Leica DM2700M Ren RL/TL microscope, employing a 50L × microscope objective (N.A. = 0.5). The SERS spectra were collected with an air-cooled charge-coupled device (CCD) detector in conjunction with a holographic grating of 1200 or 1800 lines/mm. Three lasers of the excitation wavelengths of 532, 633 or 785 nm were used for the SERS measurements.

The SERS detection of bilirubin was conducted in a phosphate buffered saline (PBS) solution or serum (10% FBS). Briefly, 200 μL of bilirubin solutions in PBS or serum of concentrations ranging from 5.0 to 500 μM were dropped onto the enPSERS biosensor. After incubation for 20 min, the enPSERS biosensor was rinsed with PBS and subsequently subject to the SERS measurements.

The SERS EF was calculated using the following equation:

$$EF = \frac{I_{SERS}}{N_{SERS}} \cdot \frac{N_{bulk}}{I_{bulk}} \quad (1)$$

where I_{SERS} and I_{bulk} represent the SERS intensity on the SERS substrates and the normal Raman intensity in the bulk solution of Raman molecules, respectively; N_{SERS} and N_{bulk} are the number of Raman molecules on the SERS substrate covered by the laser spot and the number of Raman molecules in the focal volume of the incident lasers in the absence of the SERS substrates, respectively. To calculate N_{bulk}, the following equation was used:

$$N_{bulk} = C_{RS} \bullet V \quad (2)$$

where C_{RS} is the bulk concentration of Raman molecules, and V is the focal volume of the focused incident lasers, depending on the laser wavelength. The details regarding the EF calculation can be found in the supplementary data.

3. Results and discussion

3.1. Synthesis and optimization of GO-GNS hybrids

The GO-GNS hybrids were prepared by the sequential modification of GO nanosheets with PVP and PDDA, followed by the self-assembly of plasmonic GNSs (Fig. 1A). The modification with the amphiphilic PVP molecules can remarkably improve the colloidal stability of GO nanosheets, and make the GO nanosheets more negatively charged, as demonstrated by the zeta potential change from −16.0 mV of GO nanosheets to −23.5 mV of PVP-GO nanosheets (Fig. 1B). The positively charged PDDA was exploited to further functionalize the PVP-GO nanosheets through the electrostatic attraction, leading to the zeta potential value of the PDDA-GO nanosheets positively shifting to +26.1 mV. The GNSs with the core size of 25.9 ± 3.4 nm and tip width of 18.6 ± 2.7 nm were utilized for the preparation of GO-GNS hybrids in this work (Figs. S1 and S2). The strong electrostatic interaction between the negatively charged GNSs and the positively charged PDDA-GO produced the GO-GNS hybrids. The resulting GO-GNS hybrids have a zeta potential value of +11.1 mV, much lower than that (+26.1 mV) of the PDDA-GO. The absorption spectrum of the GO-GNS hybrids shows the LSPR wavelength of 740 nm blue-shifted by ~38 nm compared with that (778 nm) of the aqueous solution of GNSs, which may be due to the electronic interaction between GNSs and GO nanosheets and the change in the dielectric constant (Lee et al., 2011) (Fig. 1C). The absorption band at ~240 nm is the feature of the GO nanosheets, clearly observed in both PDDA-GO and GO-GNS hybrids (Li et al., 2012b; Cushing et al., 2013). The loading of GNSs in the GO-GNS hybrids can be effectively controlled by the GNS amount initially added to the GO suspension (Fig. 1D). Our results show the proportional increase of the absorbance characteristic of GNSs in the GO-GNS hybrids with the GNS loading increase. There exists a positive linear relationship between the absorbance at the LSPR wavelength (740 nm) in the GO-GNS hybrids and the GNS loading. It is worth noting that a large portion of GNSs added still resided in the water phase and were not bound onto the GO nanosheets, eventually removed by the washing step. We also observed the slight red-shift of the LSPR band of the GO-GNS hybrids with the increasing GNS:GO ratio, which may be attributed to the plasmonic coupling between GNSs due to the high density of GNSs on the GO nanosheet. Fig. 1E shows two representative TEM images of GO-GNS hybrids containing the GNS:GO mass ratio of 24%

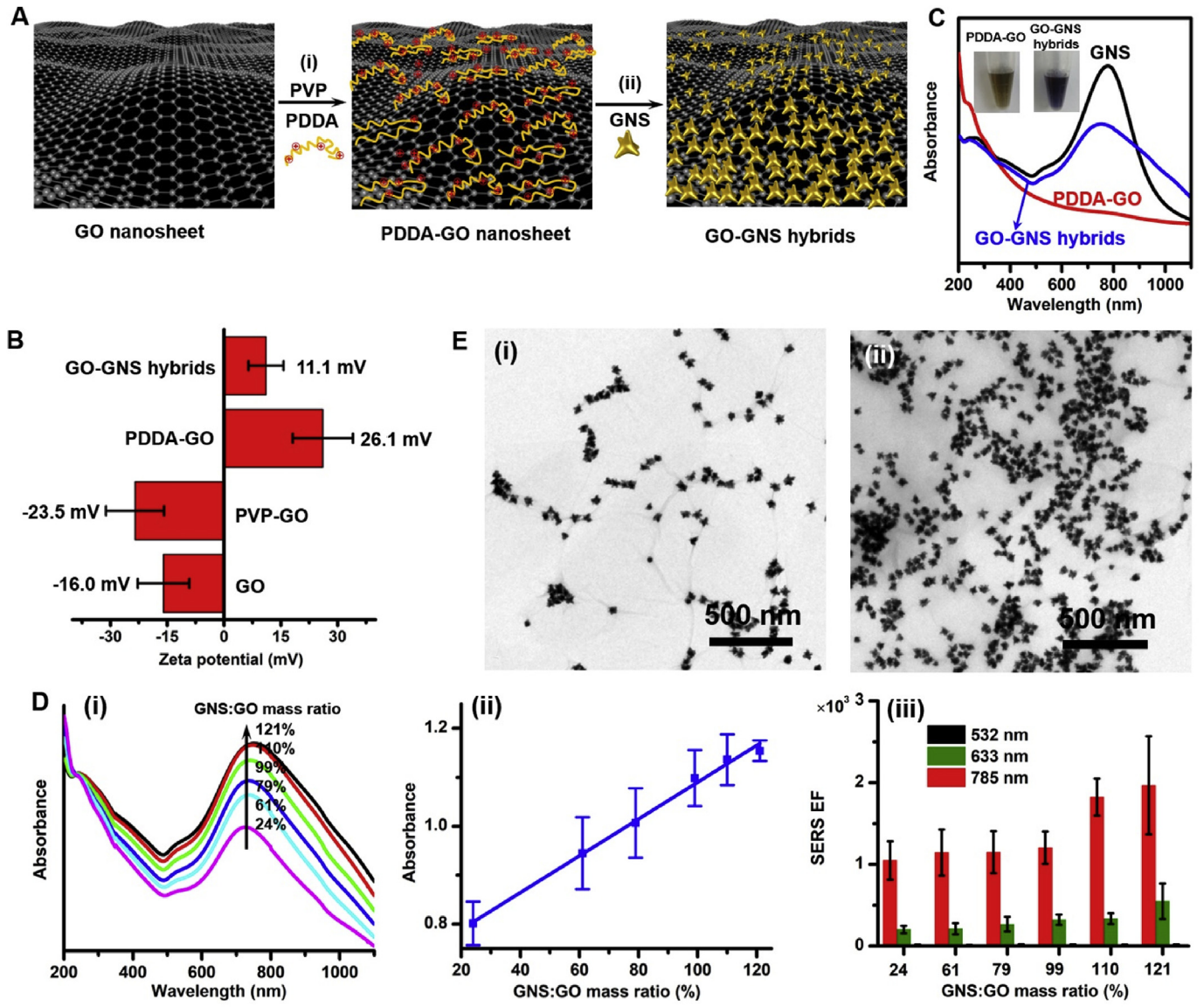

Fig. 1. Synthesis and optimization of GO-GNS hybrids. (A) Schematic illustration for the preparation of GO-GNS hybrids. (i) GO nanosheets were first functionalized with PVP and PDDA, improving the colloidal stability of GO nanosheets and endowing the GO nanosheets with the positive charges, and then (ii) GNSs were decorated on the positive charged GO nanosheets through the electrostatic interaction. (B) Zeta potential values of GO, PVP-GO, PDDA-GO and GO-GNS hybrids prepared with the GNS:GO mass ratio of 121%. (C) Absorption spectra of as-prepared GNSs, PDDA-GO and GO-GNS hybrids of 121% GNSs in water. Inset shows the optical photos of the suspensions of PDDA-GO and GO-GNS hybrids in water. (D) (i) Absorption spectra of GO-GNS hybrids containing the GNS:GO mass ratio of 24%, 61%, 79%, 99%, 110% and 121%, (ii) the corresponding absorbance at 740 nm as a function of the GNS:GO mass ratio and (iii) the corresponding SERS EFs under 532, 633 or 785 nm lasers. The detailed SERS spectra can be found in Fig. S4 of the supplementary data. (E) Representative TEM images of GO-GNS hybrids prepared with the GNS:GO mass ratio of (i) 24% and (ii) 121%.

and 121%, respectively, indicating well dispersed GNSs on the GO nanosheets (Figs. 1E and S3). The wrinkles of GO nanosheets were clearly observed around GNSs, preventing the aggregation of GNSs and providing a large number of surface-active sites for selective adsorption of biomarkers for the biosensing applications. It is obvious that the increasing addition of GNSs to the GO suspension leads to more GNSs in the hybrids, consistent with results from the absorption measurement (Fig. 1D).

To assess the effect of the GNS loading on the SERS activity of the GO-GNS hybrids, we performed the SERS measurements with 4-NTP as the Raman molecules at three different excitation wavelengths of 532, 633 and 785 nm, respectively (Fig. 1D(iii) and S4). The GO-GNS hybrids of various GO:GNS ratios were completely immersed in a solution of 1.0 μM 4-NTP, and after incubated for 2 h the GO-GNS hybrids were washed with ultrapure water. The resulting GO-GNS hybrids were subject to the SERS measurement. Very weak SERS features of 4-NTP were observed for GO-GNS hybrids with various GNS amounts at the 532 nm excitation wavelength, while the SERS intensity excited with the 633 nm or 785 nm laser is significantly stronger. To quantitatively compare the SERS activity of GO-GNS hybrids of various GNS amounts, we quantified the SERS performance through calculating the SERS EF based on the intensity of the C–S stretching band at 1081 cm^{-1} of 4-NTP (Li et al., 2015b, 2019). The SERS enhancement at 532 nm is negligible for all GO-GNS hybrids while the highest SERS EF is with the 785 nm excitation. For both 633 nm and 785 nm excitations, the SERS EF gradually increases with the increasing GNS loading. This is mainly attributed to high density GNSs dispersed on GO that favor the SERS enhancement upon the formation of more “hot-spots” between GNSs. The GO-GNS hybrids of high density GNSs may maximize the possibility of all adsorbed Raman molecules localized in the “hot spots” formed by

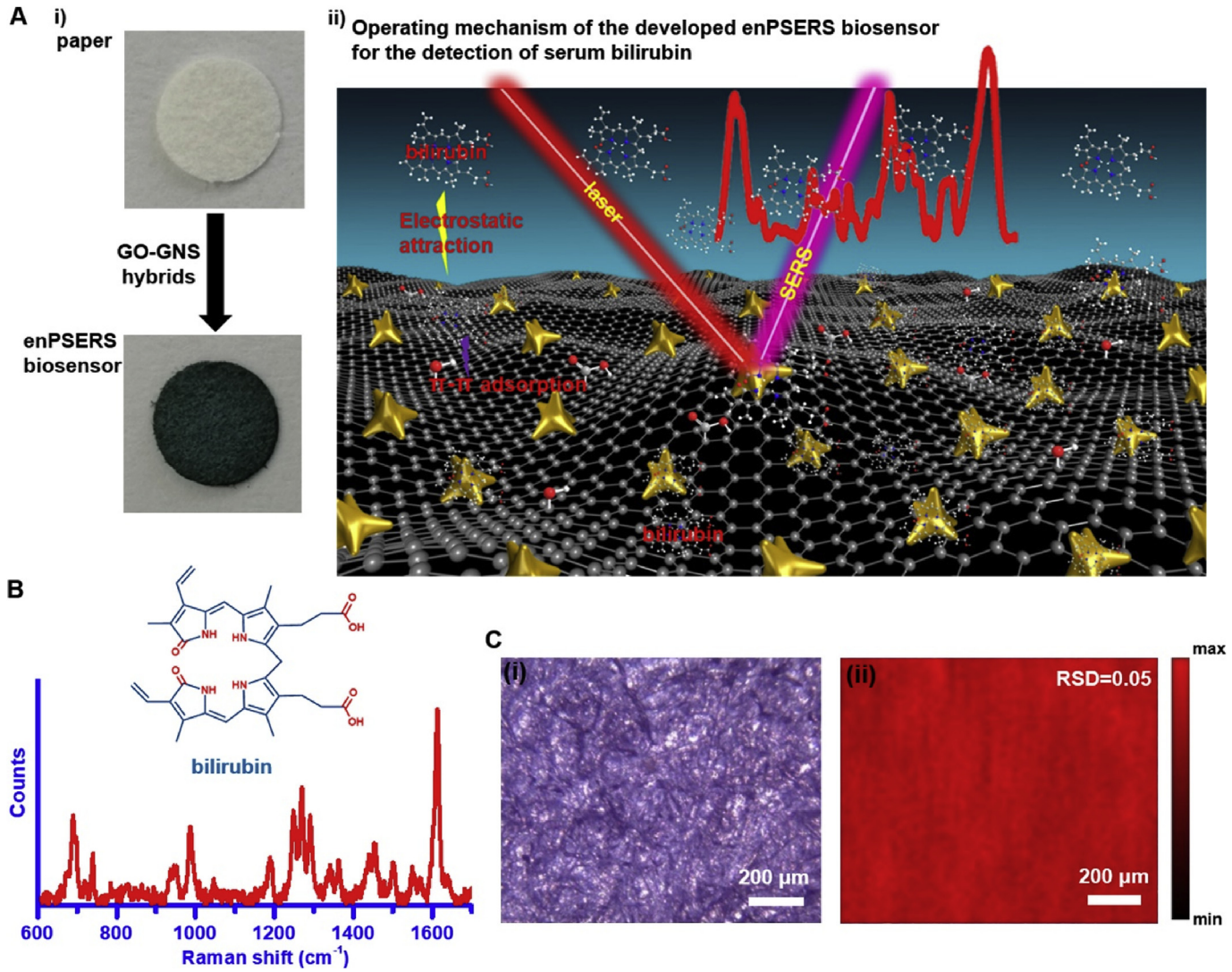

Fig. 2. Operating principle of the enPSERS biosensor for label-free detection of serum bilirubin. (A) (i) Schematic illustrating the preparation process of the enPSERS biosensor and (ii) the operating principle of the developed enPSERS biosensor for the label-free SERS detection. The enPSERS biosensor was prepared by integrating the GO-GNS hybrids into the filter paper. Simultaneous pre-concentration by the GO nanosheets and SERS enhancement by plasmonic GNSs of serum bilirubin could be achieved for the direct quantification. (B) Both molecular structure and Raman spectrum (solid) of bilirubin are shown as well (Fig. S7), assignments of which are shown in Table S1 (C) (i) Optical image and (ii) the corresponding SERS image of the enPSERS biosensor, obtained from a representative region with the aqueous solution of 4-NTP (1.0 μM) as the Raman molecules. The SERS image was created with the N–O Raman band at 1328 cm^{-1}, and the SERS intensity was normalized by the maximum SERS intensity at 1328 cm^{-1} in the data set. The SERS mapping was implemented with a step size of 20 μm over an area of 1200 μm × 1000 μm (laser: 785 nm, power on the sample: 6.57 mW, integration time: 0.1 s, objective: 5 ×). The relative standard deviation (RSD = 0.05) evidences the uniform decoration of GNSs on the GO nanosheets and thereby the high-quality of the enPSERS biosensor.

the GNSs for the huge SERS enhancement. The higher SERS EF at 785 nm results from the large overlap of the LSPR band of GNSs in the GO-GNS hybrids with the laser wavelength of 785 nm (Fig. S5). We found that the GO-GNS hybrids with the GNS:GO ratio exceeding 121% have poor dispersivity and precipitate in the suspension due to the large mass density. Thus, the GO-GNS hybrids of 121% GNSs were adopted for the following experiments.

3.2. Operating principle of the enPSERS biosensor

The commonly used laboratory filter paper consisting of uniform, microsized cellulose fibers interwoven together was employed for the preparation of the enPSERS biosensor in this work (Fig. S6). Filter paper is an ideal sensing platform for building portable miniature diagnostic devices suitable for resource-limited environments and point-of-care applications, with advantages of low-cost, easy processing, biodegradability, biocompatibility and high availability in nature (Mahadeva et al., 2015). The suspension of the GO-GNS hybrids of 121% GNS:GO mass ratio was directly dropped onto the filter paper, followed by drying at 30 °C in a vacuum oven, producing the enPSERS biosensor (Fig. 2A). With the deposition of the GO-GNS hybrids, the enPSERS biosensor appears a dark blue color. The GO-GNS hybrids possess prominent features of a large surface area, planar structure with abundant π electrons and cationic PDDA surface ligand. Previous studies showed that fluorescence was a potential issue when filter paper was used as a substrate for SERS detection (Lee et al., 2011; Li et al., 2012b; Cushing et al., 2013). However, in the present enPSERS biosensor, both GO and GNSs can be effective quenchers for the fluorescence of the filter paper, as widely reported in the literature (Shan et al., 2018). Both GO and GNSs works as effective quenchers and thus leads to negligible fluorescence emission of GO used for the preparation of the enPSERS biosensor, which could benefit the SERS detection of bilirubin (Fig. 1D). Thus, we expect that these prominent features can be utilized to enrich the anionic biomarkers through the electrostatic

and π-π interactions between the GO-GNS hybrids and the biomarkers, for the label-free SERS analysis with negligible fluorescence interference. There exist a large number of unoccupied sites on the GO nanosheets, available for the adsorption of bilirubin biomarkers. The electrostatic and π-π interactions facilitate the enhanced adsorption of bilirubin onto the unoccupied sites of the GO nanosheets, and the high-density GNSs on the GO nanosheets provide numerous "hot spots" for the huge enhancement of SERS signals of bilirubin, enabling the label-free detection of bilirubin directly in blood serum with high sensitivity and molecular specificity. Thus, it is proposed that the present enPSERS biosensor can work for high performance SERS biosensing through integrating enrichment of biomarkers by GO with SERS enhancement by the plasmonic GNSs. To evaluate the reproducibility and accuracy of the enPSERS biosensor, we performed the SERS mapping with 4-NTP as the Raman molecules and examined the uniformity of the enPSERS biosensor. The enPSERS biosensor was immersed in a solution of 4-NTP (1.0 μM), and after incubation for 2 h the enPSERS biosensor was washed with ultrapure water, followed by being subjected to the SERS mapping measurement. The SERS mapping was conducted with a step size of 20 μm over an area of 1200 μm × 1000 μm. The SERS image was constructed with the intensity of the N–O Raman band at 1328 cm^{-1}, showing uniform SERS signals over a large area (Fig. 2B). The enPSERS biosensor achieved high reproducibility, as indicated by the relative standard deviation (RSD) as low as 5%. Therefore, the present enPSERS biosensor demonstrates the excellent reproducibility for the label-free SERS detection.

3.3. Adsorption kinetics of Raman molecules

As aforementioned, the prepared GO-GNS hybrids are positively charged with the zeta potential value of +11.1 mV. To gain insights into the adsorption capability of the enPSERS biosensor toward Raman molecules of different structural features, we compared the adsorption kinetics toward neutral (uncharged) 4-NTP, positively charged MB and negatively charged TP through real-time monitoring the evolution of their respective SERS spectra excited with the 785 nm laser (Fig. 3). The experiments were performed in a customized-polydimethylsiloxane (PDMS) sample cell with a thin-quartz window to collect the SERS spectra for monitoring the adsorption process (Fig. S8). For all three Raman molecules, the intensity of SERS spectra exhibited first a monotonic increase with prolonging incubation, suggesting the progressive adsorption of these Raman molecules, and then saturated at a different time-point. The SERS response can be described as the SERS intensity ratio (I/I_{max}), where I_{max} is the maximum SERS intensity in the data set. We found that the adsorption data ($q_t = I/I_{max}$) of all three Raman molecules followed a pseudo-second-order kinetic model:

$$q_t = \frac{q_e^2 \cdot k \cdot t}{1 + q_e \cdot k \cdot t} \quad (3)$$

where q_e and q_t are the amount of Raman molecules adsorbed at equilibrium and at time t, respectively; k is the pseudo-second-order rate constant. We can clearly see that the adsorption rate constant follows the order k(TP) > k(MB) > k(4-NTP) (Fig. 3E). It is well recognized that both electrostatic and π-π interactions are two important factors affecting the adsorption of Raman molecules onto the enPSERS bionsensor. As is well-known, the electrostatic interaction that is a long-range interaction process is much stronger than the short-range π-π interaction. The electrostatic attraction causes the Raman molecules to approach the enPSERS biosensor, followed by both contributions of electrostatic and π-π interactions to the adsorption of Raman molecules. Both strong electrostatic attraction and π-π interactions exist between negatively charged TP and the enPSERS biosensor, accounting for the highest adsorption of TP onto the enPSERS biosensor; in spite of the positive charge of MB, the large aromatic structure with the strong π-π interaction may be responsible for the adsorption of MB, thus leading to much higher adsorption of MB than the uncharged 4-NTP. In addition, the large aromatic structure of MB that provides much larger Raman scattering cross-section could produce much stronger SERS signal than 4-NTP, resulting in more sensitive SERS detection of MB. Therefore, we demonstrate the excellent adsorption capability of the developed enPSERS biosensor for the negatively charged biomarkers of aromatic structures.

3.4. Label-free detection of bilirubin

The aforementioned features of the enPSERS biosensor motivated us to further explore the label-free SERS detection of bilirubin since bilirubin has similar structure (large planar structure plus carboxylic group) to that of TP. Control experiments were first performed with the bilirubin concentration of 50 μM in PBS under three different conditions: (i) on the filter paper decorated with GO alone, (ii) on the filter paper decorated with GNSs alone, and (iii) on the enPSERS biosensor (Fig. S9). The SERS intensity of bilirubin is negligible in cases of the filter paper decorated with GO or GNSs alone while much stronger with the enPSERS biosensor. This demonstrates that both the enrichment and SERS enhancement are requisite for the sensitive detection of bilirubin by the enPSERS biosensor. We further examined the time-resolved SERS spectra of bilirubin (50 μM) in PBS to gain insights into the adsorption kinetics of bilirubin on the enPSERS biosensor (Fig. 4A). In addition to the G band at 1320 cm^{-1} and D band at 1595 cm^{-1} of GO (Fig. S10) (Li et al., 2013b), the SERS spectra clearly show the characteristic Raman bands of bilirubin. The dominant SERS bands of bilirubin are at 677 cm^{-1} (twisting of C═O bond in COOH group), 716 cm^{-1} (out-of-plane ring deformation), 791 cm^{-1} (in-plane ring deformation), 936 cm^{-1} (C–H out-of-plane bending and C–CH_3 stretching), 970 cm^{-1} (methylene bridge deformation), 1048 cm^{-1} (CH_2 wagging), 1097 cm^{-1} (C–N stretching), 1117 cm^{-1} (C–C stretching and C–H deformation), 1162 cm^{-1} (CH_3 out-of-plane bending and C–C stretching), 1245 cm^{-1} (CCH bending and CCC bending), 1386 cm^{-1} (CH_3 asymmetric deformation) and 1466 cm^{-1} (C–C and C–N mixed stretching), assignments of which are also listed in Table 1 (Rai et al., 2002; Celis et al., 2016). It can be seen that the SERS intensity of the enPSERS biosensor exposed to the bilirubin solution (50 μM) with prolonging time increases rapidly for the first 50 min, followed by being saturated for the subsequent exposure. This trend closely agrees with the intensity variation of the SERS spectra for 4-NTP, MB or TP, except the different absolute SERS intensity. We immersed the enPSERS biosensor in a PBS solution for at least 24 h, and then tested the absorption spectrum of the supernatant. The absence of the absorption band characteristic of the GO-GNS hybrids in the supernatant testifies that the GO-GNS hybrids do not leave from the filter paper during the implementation of the SERS detection, indicating the high stability of the developed enPSERS biosensor (Fig. S11). The experimental data can be also fitted with the pseudo-second-order kinetic model, yielding an adsorption rate constant of 0.19 min^{-1} (Fig. 4A(ii)), a little lower than that (k = 0.23 min^{-1}) of TP.

To evaluate the sensitivity of the present enPSERS biosensor, we performed experiments with a series of bilirubin concentrations in PBS ranging from 5.0 to 500 μM (Fig. 4B). The enPSERS biosensor shows the typical G and D bands of the GO nanosheet in the absence of bilirubin. We can see that the intensity of the SERS spectra rises with the increasing concentration of bilirubin, indicating that the SERS intensity is proportional to the amount of the bilirubin adsorbed onto the enPSERS biosensor. As shown in Fig. 4B, the G band at 1320 cm^{-1} of GO has little overlap with the strong SERS band at 1245 cm^{-1} of bilirubin. Thus, it could be employed as an internal standard for the quantitative evaluation of bilirubin. To correlate the SERS measurements with the bilirubin concentration, the intensity ratio of the SERS band at 1245 cm^{-1} to the G band at 1320 cm^{-1} of GO (I_{1245}/I_{1320}) was plotted against the logarithmic concentration of bilirubin ($\log C_{BR}$) covered in this work (Fig. 4C). The SERS response (I_{1245}/I_{1320}) shows a monotonic

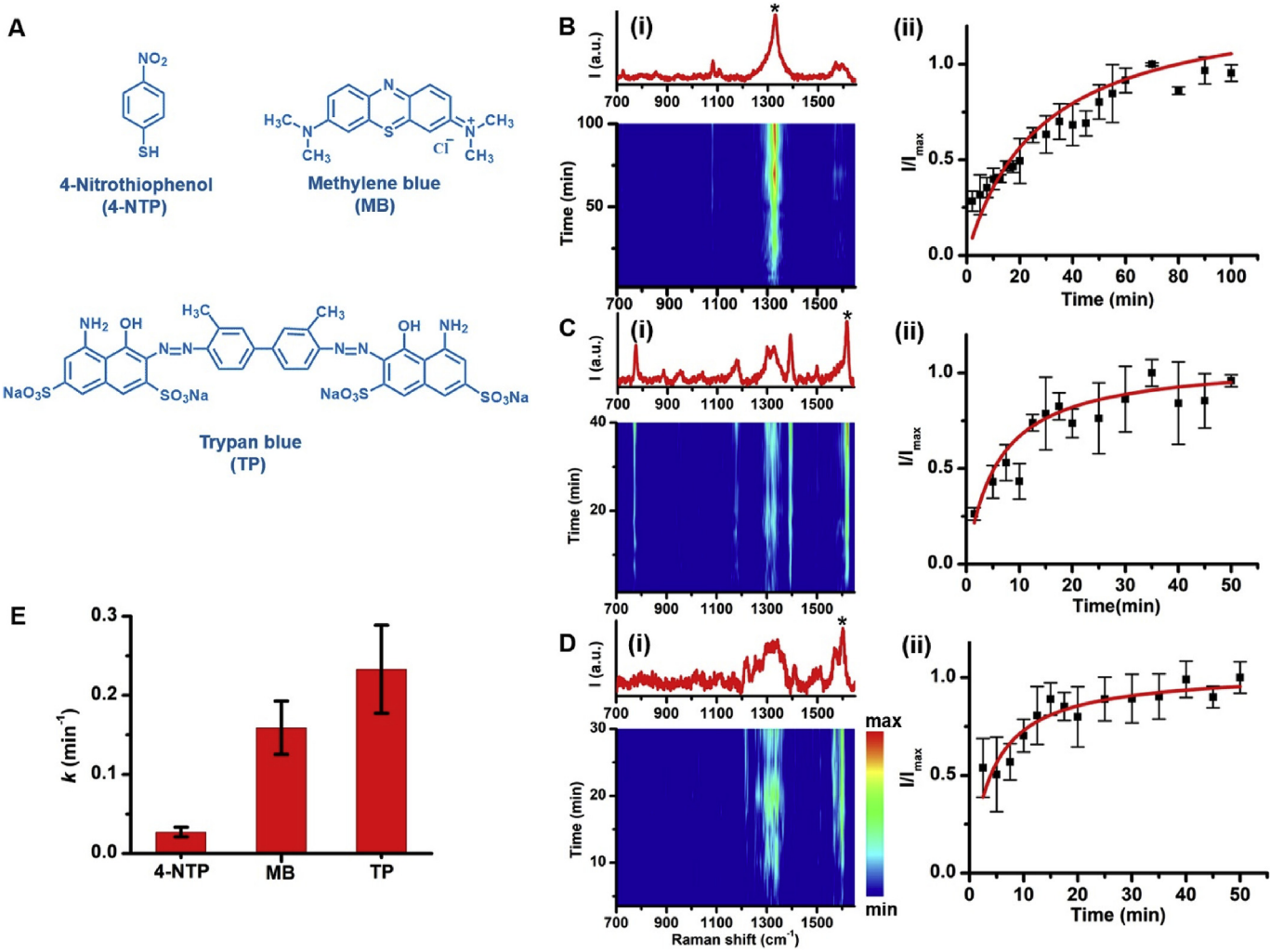

Fig. 3. Adsorption kinetics of different types of Raman molecules. (A) Molecular structures of three different types of Raman molecules investigated in this work, which are neutral (uncharged) 4-NTP, positively charged MB and negatively charged TP. (B–D) (i) Evolution of time-resolved SERS spectra and (ii) adsorption kinetic curves of the developed enPSERS biosensor toward (B) 4-NTP, (C) MB and (D) TP. The SERS measurements were implemented at the concentration of 1.0 μM for all three types of Raman molecules (laser: 785 nm, power on the sample: 0.54 mW, integration time: 1 s, objective: × 50 L). The adsorption kinetics curves (red curves in the right (ii) panels of (B–D)) were obtained through fitting the raw data with the pseudo-second-order kinetic model ($q_t = (q_e^2 \cdot k \cdot t)/(1 + q_e \cdot k \cdot t)$. The representative SERS spectra of 4-NTP, MB and TP were showed in the top of the left (i) panels), and the SERS bands (labeled with the * symbol) at 1328 cm^{-1} for 4-NTP, 1621 cm^{-1} for MB and 1603 cm^{-1} for TP were used for quantitative analysis. (E) Adsorption rate constants of the developed enPSERS biosensor for the adsorption of 4-NTP, MB and TP, obtained from the pseudo-second-order kinetic fitting. (For interpretation of the references to color in this figure legend, the reader is referred to the Web version of this article.)

increase with the increasing bilirubin concentration. Two linear regions were observed in ranges from 5.0 to 75 μM and 125–500 μM, which are fitted with the straight lines $y = 0.168 + 0.325\log C_{BR}$ ($R^2 = 0.96$) and $y = 0.253 + 0.452\log C_{BR}$ ($R^2 = 0.82$), respectively. Here, y is the intensity ratio (I_{1245}/I_{1320}) of the SERS band at 1245 cm^{-1} to the G band at 1320 cm^{-1}. The electrostatic and π-π dual-interactions may be responsible for the two linear regions. As is well-known, the electrostatic attraction is a long-range interaction process while the π-π interaction is a short-range interaction process. The electrostatic adsorption causes the bilirubin to approach the enPSERS biosensor, followed by the occurrence of the π-π interaction. We suggest that the electrostatic interaction is more important in the low concentration region for the enrichment of bilirubin, while there exist a large number of bilirubin molecules around the enPSERS biosensor in the high concentration region so that the π-π interaction may be as important as the electrostatic interaction in the high concentration region for the bilirubin adsorption with the enPSERS biosensor. We computed the limit of detection (LOD) according to the IUPAC definition: $LOD = 3\sigma/s$, where σ and s represent the standard deviation of blank measurements and the slope of the linear equation in the low concentration region of 5.0–75 μM, respectively. The LOD of the present enPSERS biosensor is 0.223 μM for detection of bilirubin in PBS. The I_{1245}/I_{1320} value gave a relative standard deviation (RSD) of 3.6–8.9% over the bilirubin concentration range investigated. The low RSD values suggest the excellent reproducibility of the present enPSERS biosensor for detection of bilirubin.

3.5. Detection of bilirubin in spiked serum samples

To test the applicability of the present enPSERS biosensor, detection of bilirubin in serum samples was conducted with various concentrations of bilirubin spiked into serum (10% FBS) (Fig. 5). In this study, FBS employed as the blood serum has no detectable bilirubin level. Additional procedure is not needed to remove the biological substances such as proteins, nucleic acids, cholesterol, glucose and sodium in blood serum prior to the SERS measurements. Fig. 5A shows the SERS spectra of the enPSERS biosensor in the presence of various concentrations of bilirubin in blood serum. We noted the subtle spectral difference

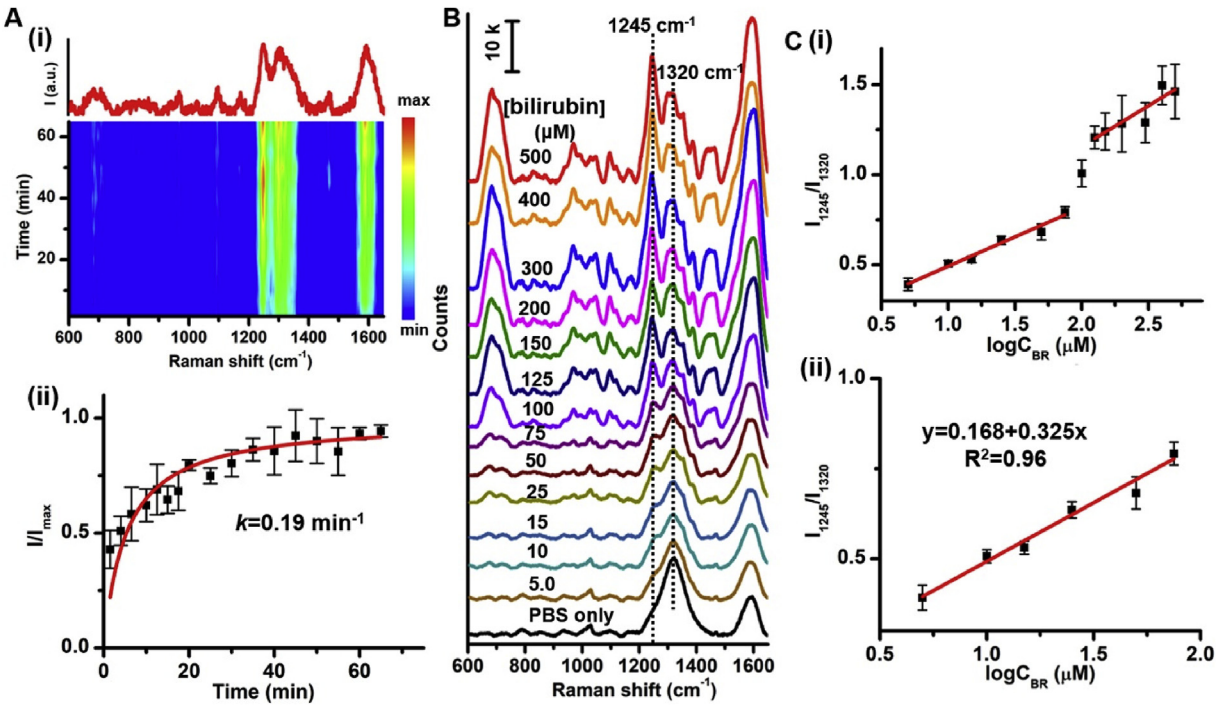

Fig. 4. Label-free SERS detection of bilirubin in PBS. (A) (i) Time-resolved SERS spectra and (ii) the SERS intensity of the 1245 cm^{-1} Raman band as a function of incubation time of the enPSERS biosensor in the presence of 50 μM bilirubin in PBS. The top panel in A(i) is the averaged SERS spectrum over the measurement period. (B) SERS spectra of the enPSERS biosensor in the absence or presence of various concentrations of bilirubin in PBS ranging from 5.0 to 500 μM. (C) (i) The plot of the I_{1245}/I_{1320} intensity ratio as a function of the logarithmic concentration of bilirubin in PBS and (ii) the zoom-in linear region in the low concentration region (5.0–75 μM) of the I_{1245}/I_{1320} - logC_{BR} curve. All experiments were performed in triplicates, and the error bars at each concentration of bilirubin represent the standard deviation of the I_{1245}/I_{1320} intensity ratio from independent experiments. The SERS measurements were conducted with the laser of 785 nm, laser power on the sample of 1.04 mW, exposure time of 1 s, and 10 accumulations.

between PBS and serum, resulting from the background subtraction rather than distinct composition (Fig. S12). Obviously, the SERS intensity gradually increases upon addition of elevated concentrations of bilirubin. Similarly, the plot of I_{1245}/I_{1320} against the logarithmic concentration of bilirubin reveals two linear regions that are fitted as $y = 0.200 + 0.200\log C_{BR}$ ($R^2 = 0.99$) from 5.0 to 150 μM and $y = 4.058 + 2.166\log C_{BR}$ ($R^2 = 0.99$) from 150 to 500 μM, respectively (Fig. 5B). The RSD values are between 0.3% and 12.4% over the concentration range investigated, indicating excellent reproducibility even in blood serum. The LOD value is calculated to be 0.436 μM by the linear equation in the low concentration region, a little higher than that (0.223 μM) in PBS. As is well-known, serum albumin could bind to free bilirubin with high affinity, forming water-soluble bilirubin complexes (Brodersen and Stern, 1980); however, these substances existing in blood serum have only little effect on the label-free SERS detection of free bilirubin in the present enPSERS biosensor. Biological substances in blood serum with structures similar to neutral 4-NTP and positively charged MB have low adsorption on the enPSERS biosensor; thus, little influence of these biological substances may be accounted for their low adsorption and small Raman scattering cross-sections. In addition, the low sensitivity of the SERS detection of serum bilirubin was observed when colloidal GNSs were used alone (Fig. S13). Thus, the experimental results above prove that the present enPSERS biosensor exhibits excellent detection performance and can work for the detection of free bilirubin in blood serum.

To validate the practical exploitation of the present method, we further tested three samples obtained by spiking free bilirubin into the blood serum, results of which were compared with those from the commercial diazo reaction method (Table 2 and Fig. S14). We can clearly see that results obtained from both methods are comparable with negligible difference. The recovery percentage is acceptable in the clinical range, calculated by $(C_2–C_0)/C_1 \times 100\%$, where C_0, C_1 and C_2 are the concentrations of bilirubin in the initial blood serum ($C_0 = 0$), in nominally spiked serum samples and tested by the present enPSERS biosensor, respectively. In addition, the usage of the ratio of the bilirubin:GO Raman intensity for the quantification detection of bilirubin will improve the detection accuracy of the present biosensor, excluding the effect of the external environments and measurement conditions. Therefore, the developed enPSERS biosensor can work for the label-free detection of free bilirubin directly in blood serum for the jaundice diagnosis, with high sensitivity, specificity, simplicity, rapidity and accuracy. The excellent performance was derived from the following

Table 1
Assignments of SERS bands of bilirubin (Rai et al., 2002; Celis et al., 2016).

Raman shift (cm^{-1})	Assignment	Raman shift (cm^{-1})	Assignment
677	Twisting of C=O bond in COOH group	1097	C–N stretching
716	Out-of-plane ring deformation	1117	C–C stretching and C–H deformation
791	In-plane ring deformation	1162	CH_3 out-of-plane bending and C–C stretching
936	C–H out-of-plane bending and C–CH_3 stretching	1245	CCH bending and CCC bending
970	Methylene bridge deformation	1386	CH_3 asymmetric deformation
1048	CH_2 wagging	1466	C–C and C–N mixed stretching

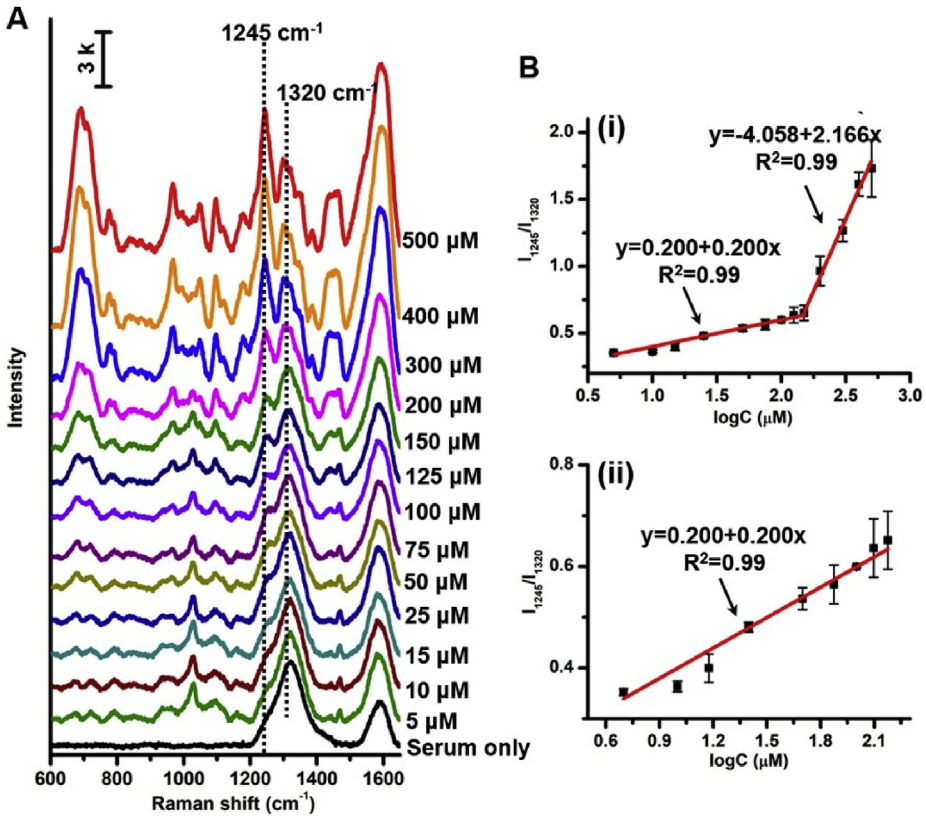

Fig. 5. Label-free SERS detection of bilirubin in blood serum. (A) SERS spectra of the enPSERS biosensor upon addition of serum only and various concentrations of bilirubin in blood serum ranging from 5.0 to 500 μM. (B) (i) Plot of the I_{1245}/I_{1320} ratio against the logarithmic concentration of bilirubin investigated, and (ii) the calibration curve of the I_{1245}/I_{1320}–logC_{BR} curve at the low concentration region. The SERS measurements were conducted with the laser of 785 nm, laser power on the sample of 1.04 mW, exposure time of 1 s, and 10 accumulations.

Table 2
Comparison of quantification results of serum bilirubin in spiked blood serum samples measured by the developed enPSERS biosensor and the commercial diazo reaction method.

Sample no.	Spiked [bilirubin] (μM)	enPSERS biosensor			Diazo reaction method (μM)
		Tested (μM)	Recovery	RSD	
1	268	245.4	91.6%	10.2%	248.2
2	58	53.7	92.6%	15.6%	55.5
3	13	10.7	82.3%	13.1%	13.6

contributions: (i) high enrichment capability through the electrostatic and π-π interactions between the bilirubin and GO-GNS hybrids, (ii) the superquenching of fluorescence by both GO and GNSs, and (iii) the high SERS enhancement of intrinsic Raman signals of bilirubin by GNSs. Unlike other traditional methods such as colorimetric, fluorescent and electrochemical methods, the present enPSERS biosensor exploits the intrinsic SERS signatures of bilirubin for its quantification, which provides excellent specificity and less interference from the complicated biological matrices. Therefore, all of these excellent features make this method apply well to rapidly screening or diagnosis of jaundice.

4. Conclusions

In summary, we have developed a paper-based SERS biosensor named enPSERS biosensor, that could be used for label-free SERS detection of free bilirubin in blood serum. The developed biosensor comprises GO-GNS hybrids decorated onto the filter paper, which integrates the high sensitivity of the SERS detection, enrichment for bilirubin and fluorescence quenching capability of the GO-GNS hybrids for sensitive, label-free SERS detection of serum bilirubin. The sensing strategy was mainly based on the strong adsorption of the bilirubin biomarkers and the subsequent SERS enhancement of the intrinsic SERS signatures of bilirubin. Results show that the adsorption process follows the pseudo-second-order kinetics with the adsorption rate constant in the order of k(4-NTP) < k(MB) < k(TP). We confirm that the SERS enhancement can be effectively controlled by the loading of GNSs. The developed enPSERS biosensor shows two differential linear response ranges from 5.0 to 150 μM and 150–500 μM for the detection of free bilirubin in blood serum with the LOD as low as 0.436 μM. The results of SERS detection of bilirubin in blood serum were comparable to that in PBS. Although there exist a large number of biological substances in human serum, little effect on the detection of serum bilirubin is observed. The comparison of the results obtained from our present enPSERS biosensor with the commercial diazo reaction method for determination of free bilirubin in blood serum reveals the clinical effectiveness and suitability of the developed paper-based SERS biosensor. With the features of high sensitivity, rapidness, simplicity and excellent specificity, the present SERS biosensor for the label-free detection of serum bilirubin holds considerable promise for clinical translation in accurate diagnosis of jaundice and its related diseases.

CRediT authorship contribution statement

Xiang Pan: Conceptualization, Data curation, Formal analysis, Investigation, Methodology, Writing - review & editing. **Linhu Li:** Investigation, Methodology, Project administration, Resources, Writing - review & editing. **Jiayi Tan:** Investigation, Writing - review & editing. **Haitao Wang:** Investigation, Writing - review & editing. **Mengling Liao:** Investigation, Writing - review & editing. **Caiju Chen:** Investigation, Writing - review & editing. **Beibei Shan:** Investigation, Methodology, Project administration, Resources, Writing - review & editing. **Yingfan Chen:** Investigation, Writing - review & editing. **Ming Li:** Conceptualization, Data curation, Formal analysis, Funding acquisition, Investigation, Methodology, Project administration, Writing - original draft, Writing - review & editing.

Declaration of competing interest

The authors declare that they have no known competing financial interests or personal relationships that could have appeared to influence the work reported in this paper.

Acknowledgements

The authors would like to acknowledge financial support by the National Thousand Young Talents Program of China, National Natural Science Foundation of China (No. 51871246), Innovation-Driven Project of Central South University (No. 2018CX002) and Hunan Provincial Science & Technology Program (No. 2017XK2027).

Appendix A. Supplementary data

Supplementary data to this article can be found online at https://doi.org/10.1016/j.bios.2019.111713.

References

Ameri, M., Schnaars, H., Sibley, J., Honor, D., 2011. J. Vet. Diagn. Investig. 23 (1), 120–123.
Bai, X., Wang, L., Ren, J.Q., Bai, X., Zeng, L., Shen, A., Hu, J.M., 2019. Anal. Chem. 91 (4), 2955–2963.
Batra, B., Lata, S., Rana, J.S., Pundir, C.S., 2013. Biosens. Bioelectron. 44, 64–69.
Berthelot, P., Duvaldestin, P., Fevery, J., 2018. Physiology and disorders of human bilirubin metabolism. In: Heirwegh, K.,P.M. (Ed.), Bilirubin. CRC Press, Boca Raton, pp. 173–214.
Bhutani, V.K., Johnson, L.H., Gourley, G., 2003. Pediatrics 111 (4), 919–920.
Bonnett, R., Davies, J.E., Hursthouse, M.B., 1976. Nature 262, 326–328.
Brito, M.A., Silva, R.F., Brites, D., 2006. Clin. Chim. Acta 374 (1–2), 46–56.
Brodersen, R., Stern, L., 1980. Crit. Rev. Clin. Lab. Sci. 11 (4), 307–399.
Brolo, A.G., Arctander, E., Gordon, R., Leathem, B., Kavanagh, K.L., 2004. Nano Lett. 4 (10), 2015–2018.
Celis, F., Campos-Vallette, M.M., Gómez-Jeria, J.S., Clavijo, R.E., Jara, G.P., Garrido, C., 2016. Spectrosc. Lett. 49 (5), 336–342.
Chen, S., Li, X., Zhao, Y., Chang, L., Qi, J., 2015. Carbon 81, 767–772.
Chen, Y., Zhang, Y., Pan, F., Liu, J., Wang, K., Zhang, C., Cheng, S., Lu, L., Zhang, W., Zhang, Z., Zhi, X., 2016. ACS Nano 10 (9), 8169–8179.
Cushing, S.K., Li, M., Huang, F., Wu, N., 2013. ACS Nano 8 (1), 1002–1013.
Doumas, B.T., Perry, B., Jendrzejczak, B., Davis, L., 1987. Clin. Chem. 33 (8), 1349–1353.
Du, Y., Li, X., Lv, X., Jia, Q., 2017. ACS Appl. Mater. Interfaces 9 (36), 30925–30932.
Ellairaja, S., Shenbagavalli, K., Ponmariappan, S., Vasantha, V.S., 2017. Biosens. Bioelectron. 91, 82–88.
Fan, Z., Kanchanapally, R., Ray, P.C., 2013. J. Phys. Chem. Lett. 4 (21), 3813–3818.
Fang, Y., Guo, S., Zhu, C., Zhai, Y., Wang, E., 2010. Langmuir 26 (13), 11277–11282.
Han, X.X., Schmidt, A.M., Marten, G., Fischer, A., Weidinger, I.M., 2013. ACS Nano 7 (4), 3212–3220.
Hajzer, Š., 1989. Clin. Chem. Lab. Med. 27 (7), 445–450.
Hooda, V., Gahlaut, A., Gothwal, A., Hooda, V., 2017. Biotechnol. Lett. 39 (10), 1453–1462.
Hutchinson, D.W., Johnson, B., Knell, A.J., 1972. Biochem. J. 127 (5), 907–908.
Kazmierczak, S.C., Robertson, A.F., Catrou, P.G., Briley, K.P., Kreamer, B.L., Gourley, G.R., 2002. Clin. Chem. 48 (7), 1096–1097.
Lee, C.H., Hankus, M.E., Tian, L., Pellegrino, P.M., Singamaneni, S., 2011. Anal. Chem. 83 (23), 8953–8958.
Li, J.F., Zhang, Y.J., Ding, S.Y., Panneerselvam, R., Tian, Z.Q., 2017. Chem. Rev. 117 (7), 5002–5069.
Li, L., Liao, M., Chen, Y., Shan, B., Li, M., 2019. J. Mater. Chem. B 7 (5), 815–822.
Li, M., Cushing, S.K., Zhang, J., Lankford, J., Aguilar, Z.P., Ma, D., Wu, N., 2012a. Nanotechnology 23, 115501.
Li, M., Cushing, S.K., Zhou, X., Guo, S., Wu, N., 2012b. J. Mater. Chem. 22 (44), 23374–23379.
Li, M., Zhang, J., Suri, S., Sooter, L.J., Ma, D., Wu, N., 2012c. Anal. Chem. 84, 2837–2842.
Li, M., Cushing, S.K., Zhang, J., Suri, S., Evans, R., Petros, W.P., Gibson, L.F., Ma, D., Liu, Y., Wu, N., 2013a. ACS Nano 7, 4967–4976.
Li, M., Zhou, X., Ding, W., Guo, S., Wu, N., 2013b. Biosens. Bioelectron. 41, 889–893.
Li, M., Kang, J.W., Dasari, R.R., Barman, I., 2014. Angew. Chem. Int. Ed. 53, 14115–14119.
Li, M., Cushing, S.K., Wu, N., 2015a. Analyst 140, 386–406.
Li, M., Kang, J.W., Sukumar, S., Dasari, R.R., Barman, I., 2015b. Chem. Sci. 6 (7), 3906–3914.
Lu, G., Li, H., Liusman, C., Yin, Z., Wu, S., Zhang, H., 2011. Chem. Sci. 2 (9), 1817–1821.
Mahadeva, S.K., Walus, K., Stoeber, B., 2015. ACS Appl. Mater. Interfaces 7 (16), 8345–8362.
Olusanya, B.O., Kaplan, M., Hansen, T.W., 2018. Lancet Child Adolesc. Health 2 (8), 610–620.
Panikar, S.S., Ramírez-García, G., Sidhik, S., Lopez-Luke, T., Rodriguez-Gonzalez, C., Ciapara, I.H., Castillo, P.S., Camacho-Villegas, T., De la Rosa, E., 2018. Anal. Chem. 91 (3), 2100–2111.
Pu, Y., Zhao, Y., Zheng, P., Li, M., 2018. Inorg. Chem. 57, 8599–8607.
Qiu, X., You, X., Chen, X., Chen, H., Dhinakar, A., Liu, S., Guo, Z., Wu, J., Liu, Z., 2017. Int. J. Nanomed. 12, 4349–4360.
Rahman, M.A., Lee, K.S., Park, D.S., Won, M.S., Shim, Y.B., 2008. Biosens. Bioelectron. 23 (6), 857–864.
Rai, A.K., Rai, S.B., Rai, D.K., Singh, V.B., 2002. Spectrochim. Acta 58 (10), 2145–2152.
Rolinski, B., Küster, H., Ugele, B., Gruber, R., Horn, K., 2001. Clin. Chem. 47 (10), 1845–1847.
Rycenga, M., Cobley, C.M., Zeng, J., Li, W., Moran, C.H., Zhang, Q., Qin, D., Xia, Y., 2011. Chem. Rev. 111 (6), 3669–3712.
Shan, B., Pu, Y., Chen, Y., Liao, M., Li, M., 2018. Coord. Chem. Rev. 371, 11–37.
Silbernagl, S., Despopoulos, A., 2009. Color atlas of physiology. In: Nutrition and Digestion, sixth ed. Georg Thieme Verlag KG, Stuttgart, pp. 252.
Stiles, P.L., Dieringer, J.A., Shah, N.C., Van Duyne, R.P., 2008. Annu. Rev. Anal. Chem. 1, 601–626.
Subbiah, V., West, H.J., 2016. JAMA Oncol. 2 (8) 1103-1103.
Thangamuthu, M., Gabriel, W., Santschi, C., Martin, O., 2018. Sensors 18 (3), 800.
Wang, Y., Yan, B., Chen, L., 2012. Chem. Rev. 113 (3), 1391–1428.
Wang, Z., Zong, S., Wu, L., Zhu, D., Cui, Y., 2017. Chem. Rev. 117 (12), 7910–7963.
Wang, P., Xia, M., Liang, O., Sun, K., Cipriano, A.F., Schroeder, T., Liu, H., Xie, Y.H., 2015. Anal. Chem. 87 (20), 10255–10261.
Wei, W., Li, S., Millstone, J.E., Banholzer, M.J., Chen, X., Xu, X., Schatz, G.C., Mirkin, C.A., 2009. Angew. Chem. Int. Ed. 48 (23), 4210–4212.
Xu, W., Ling, X., Xiao, J., Dresselhaus, M.S., Kong, J., Xu, H., Liu, Z., Zhang, J., 2012. Proc. Natl. Acad. Sci. U. S. A 109 (24), 9281–9286.
Yu, X., Cai, H., Zhang, W., Li, X., Pan, N., Luo, Y., Wang, X., Hou, J.G., 2011. ACS Nano 5 (2), 952–958.
Yuan, C., Deng, Y., Li, X., Li, C., Xiao, Z., Liu, Z., 2018. Anal. Chem. 90 (13), 8178–8187.
Zeng, B., LIu, Z., Zhou, X., 1994. Anal. Sci. 10 (1), 95–99.
Zhang, H., Harpster, M.H., Wilson, W.C., Johnson, P.A., 2012. Langmuir 28 (8), 4030–4037.
Zhou, J., Xiong, Q., Ma, J., Ren, J., Messersmith, P.B., Chen, P., Duan, H., 2016. ACS Nano 10 (12), 11066–11075.